HHS Public Access

Author manuscript

Nat Plants. Author manuscript; available in PMC 2017 October 13.

Published in final edited form as:

Nat Plants. ; 3: 17010. doi:10.1038/nplants.2017.10.

Structure of the SHR-SCR heterodimer bound to the BIRD/IDD transcriptional factor JKD

Yoshinori Hirano[1], **Masahiro Nakagawa**[1], **Tomoe Suyama**[1], **Kohji Murase**[1,2], **Maya Shirakawa**[1], **Seiji Takayama**[2,3], **Tai-ping Sun**[4], and **Toshio Hakoshima**[1]

[1]Structural Biology Laboratory, Nara Institute of Science and Technology, 8916-5 Takayama, Ikoma, Nara 630-0192, Japan

[2]The laboratory of Intercellular communication, Nara Institute of Science and Technology, 8916-5 Takayama, Ikoma, Nara 630-0192, Japan

[4]Department of Biology, Duke University, Durham, NC 27708, USA

Abstract

The plant-specific GAI-RGA-and-SCR (GRAS) family proteins play critical roles in plant development and signaling. Two GRAS proteins, SHORT-ROOT (SHR) and SCARECROW (SCR), cooperatively direct asymmetric cell division and the patterning of root cell types by transcriptional control in conjunction with BIRD/INDETERMINATE DOMAIN (IDD) transcription factors, although precise details of these specific interactions and actions remain unknown. Here, we present the crystal structures of the SHR-SCR binary and JKD/IDD10-SHR-SCR ternary complexes. Each GRAS domain comprises one α/β core subdomain with an α-helical cap that mediates hetero-dimerization by forming an intermolecular helix bundle. The α/β core subdomain of SHR forms the BIRD-binding groove, which specifically recognizes the zinc fingers of JKD. We identified a conserved SHR-binding motif (SHBM) in 13 BIRD/IDD transcription factors. Our results establish a structural basis for GRAS-GRAS and GRAS-BIRD interactions and provide valuable clues towards our understanding of these regulators involved in plant-specific signaling networks.

GRAS proteins are plant-specific key regulators of transcription in diverse processes including root development, gibberellin signal transduction and phytochrome signaling. Two GRAS proteins, SHR and SCR, function as central regulators in the radial patterning of *Arabidopsis* roots [1,2]. Mutations in *SCR* and *SHR* genes lead to the disruption of asymmetric cell division of the cortex/endodermis initial (CEI) [3-6] and defects in the stem cell niche at

Correspondence and requests for materials should be addressed to: T. Hakoshima, Structural Biology Laboratory, Nara Institute of Science and Technology, 8916-5 Takayama, Ikoma, Nara 630-0192, Japan. Tel.: +81-743-72-5570; Fax: +81-743-72-5579.
[3]Present address: Department of Applied Biological Chemistry, The University of Tokyo, 1-1-1 Yayoi, Bunkyo-ku, Tokyo 113-8657, Japan

Author Contributions: Y. H. and T. H. conceived and designed the project. Y. H. was responsible for construct design for the protein preparations. M. S., Y. H. and M. N. prepared the DNA constructs. Y. H., M. N. and T. S. performed protein biochemistry, crystallization and X-ray data collection. Y. H. solved and refined the structures. K. M. performed *in vivo* binding assay supervised by S.T. Y. H., M. N., T. S. and T. H. interpreted data. Y. H., T.P.S and T. H. wrote the manuscript.

Additional information: Supplementary information is available online.

Competing interests: The authors declare no competing financial interests.

the quiescent center (QC) [7]. SHR and SCR also contribute to bundle sheath cell fate in leaves [8], suggesting that their function is not limited to root. SHR is a mobile transcription regulator, which is transcribed in the stele, but moves into the adjacent cell layer where SCR sequesters SHR to the nucleus by forming SHR-SCR heterodimer through conserved GRAS domains [9-11]. Subsequently, the SHR-SCR complex up-regulates *SCR* expression to activate a positive *SCR* transcription loop, which prevents SHR movement out of the single endodermis cell layer [10-12]. The SHR-SCR complex up-regulates several genes encoding zinc finger (ZF) transcription factors of the BIRD/INDETERMINATE DOMAIN (IDD) family [11-13] and cell cycle regulator CYCLIN D6 [14]. Several members of the BIRD/IDD family (*e.g.*, JACKDAW [JKD]/IDD10, BALDIBIS [BIB], MAGPIE [MGP]/IDD3) are required for asymmetric cell division of ground tissue and QC specification by direct protein-protein interaction with SHR and/or SCR to control ground tissue patterning during root growth [15-17]. However, the binding modes and the molecular mechanisms by which this interplay occurs remain unknown. Here, we report the structures of the SHR-SCR heterodimer and the JKD-SHR-SCR complex. Our structural and biochemical analyses indicate that SHR-SCR function as transcription cofactors by binding to the third and fourth ZFs, (ZF3-ZF4) of JKD out of the N-terminal four ZFs (ZF1 to ZF4) *via* a specific groove in SHR, and that the ZF1-ZF2-ZF3 of JKD in the JKD-SHR-SCR complex is involved in DNA binding.

Results

Structural determination of the SHR-SCR complex

GRAS proteins comprise a variable N-terminal region and a conserved C-terminal GRAS domain (Fig. 1a) [18,19]. The N-terminal regions are predicted to be intrinsically disordered without their interaction partners, as demonstrated in the structural work of the N-terminal DELLA domain of another *Arabidopsis* GRAS protein GAI bound to the gibberellin (GA) receptor GID1 [20,21]. The GRAS domain-containing fragments of SHR (residues 59-531) and SCR (275-653) were co-expressed in *E. coli* cells and the purified protein sample was shown to exist as a stable heterodimer in solution by our analytical ultracentrifugation (AUC) (Fig. 1b). We determined the crystal structure of the binary complex, hereafter referred to as the SHR-SCR complex, at 2.0 Å resolution (Supplementary Table 1). The GRAS domains display similar globular structures and form a head-to-head 1:1 heterodimer, which has a pseudo-dyad axis between the GRAS domains (Fig. 1c). Most of the N-terminal extensions were not observed in the current electron density map, whereas the short N-terminal segment of SHR, the N-terminal strap, was observed to extend towards SCR (Fig. 1c, in red).

GRAS domain architecture

Each GRAS domain includes an α-helical cap and α/β core subdomains comprising a total of seventeen helices (fourteen α- and three 3_{10} helices for SHR) and nine (β-strands (Fig. 1c,d, Supplementary Fig. 1a). Each α-helical cap of SHR and SCR comprises six helices (the N-terminal α1-α3 and αA helices and the α10-α11 helices extending from the α/β core) and form a helix bundle structure, whereas αA helix in SHR is unfolded and folded into a short 3_{10} helix in SCR (ηA in Fig. 1c, 2a). The α/β core subdomain incorporates a nine-stranded mixed (β-sheet with three α-helices on one side and four α-helices on the

other side. Overlay of the α/β cores of SHR and SCR shows superimposition with local deviations found in the deletion/insertion-containing regions (β2–α7 loop, η2 helix/β4–α9 loop and η3 helix/α11–α12 loop) (Fig. 2b), which display relatively poor sequence homology (Supplementary Fig. 1a-c). These regions are located at the boundary region between the α-helical cap and α/β core subdomains and responsible for a large shift in the orientation of the α-helical cap relative to the α/β core (Fig. 2c). As the α-helical caps mediate dimerization (Fig. 1c), the shift in α-helical cap orientation results in a small asymmetric deviation of the SHR-SCR dimer.

The GRAS domains are characterized by leucine heptad repeats I and II (LHRI and LHRII, respectively), and conserved sequence motifs, VHIID, PFYRE and SAW [18] (Fig. 1a). In our structure, the VHIID and SAW sequences are located at the β1and β9 strands of the α/ β core, respectively. The Pro residue of PFYRE is located at the α9-β5 loop, while the other residues at the α10 and α11 helices of the cap (Fig. 2d, e). These residues seem to contribute to maintaining the three-dimensional structure and mutations/deletion of these residues may induce unfolding and/or structural instability resulting in dysfunction [22].

The GRAS domains of SHR and SCR share structural similarity with the α/β folds of *S*-adenosyl methionine-dependent methyltransferases (SAM-MTs) (Supplementary Fig. 2a-e). The central (β-sheet of SAM-MT comprising seven (β-strands [23] superimposes well on the GRAS domain, while GRAS domains possess an extra module (β6 and (β7 strands and α13 helix) at one side of the central (β-sheet (Fig. 1d). This GRAS-specific extra module of SHR is found to participate in direct interactions with the zinc finger of JKD (see below). As with SAM-MTs, GRAS domains possess a cavity in the α/β core covered by the α-helical cap (Supplementary Fig. 3). However, GRAS domains lack the SAM-binding motifs, which are conserved in SAM-MTs and located inside the cavity (frequently found in the loops following the β1, β2 and β3 strands) [23,24] (Supplementary Fig. 2f). We did not detect any binding of SHR-SCR to either SAM or *S*-adenosyl homocysteine, or the product monomethyl-L-lysine, in our binding assays using isothermal titration calorimetry (ITC) (Supplementary Fig. 4). Taken together, we concluded that the GRAS domain possesses no methyltransferase activity.

The SHR-SCR interface

Dimerization of the GRAS domains of SHR and SCR is mediated by the α-helical caps, which form an interface area comprising a large buried accessible surface area (~2,070 Å^2). At the interface, eight helices (α2, α3, αA/ηA and α11 helices) and four loops (α2-α3 and α10-α11 loops) from both α-helical caps are involved in direct interactions to engage with each other (Fig. 3a). The electrostatic surface potentials of SHR are positively-charged and complementary with the negatively-charged surface of SCR (Fig. 3b). The interface incorporates polar interactions forming direct hydrogen bonds and salt bridges, and also water-mediated hydrogen bonds (Fig. 3c, d).

The interface also contains nonpolar contacts. Notably, the SCR nonpolar segment encompassing the C-terminal half of α3 helix followed by α3-ηA loop and short 3_{10}-helix ηA acts as a “hydrophobic belt”, which wraps around α2 helix from SHR with nonpolar contacts (Fig. 3e). The hydrophobic belt is conserved in SCR beyond species but not in other

GRAS proteins (Supplementary Fig. 1). Nonpolar residues at the SHR α2 helix are also conserved and specific for SHR. These interactions may contribute towards conferring specificity on the hetero-dimerization between SHR and SCR. In SHR, most of the long α3-ηA loop is folded into the αA helix, which makes a parallel helix-helix interaction with α2 helix from SCR (Fig. 1c). Thus, the interface contains asymmetric interactions, which may confer specificity. Mutations of both nonpolar and polar residues located at the SHR-SCR interface reduce binding affinity (Fig. 3f). The N-terminal extension (red in Fig. 3a) of SHR wraps around SCR but has no significant contribution towards SHR-SCR binding affinity (Fig. 3f). The observed SHR-SCR interactions in our crystal were also supported by the *in vivo* binding assay using *Nicotiana benthamiana* leaves (Fig. 3g, Supplementary Fig. 5b) and yeast two-hybrid assay (Supplementary Fig. 5a).

Zinc fingers ZF3 and ZF4 directly bind the SHR-SCR complex

BIRD/IDD transcription factors contain four conserved zinc fingers (ZFs) at the N-terminal regions, with the first two (ZF1 and ZF2) of the C_2H_2 type ZF and the next two (ZF3 and ZF4) of the C_2HC type (Supplementary Fig. 6). Previous yeast two-hybrid analyses suggested that the N-terminal ZF region of MGP and JKD is responsible for directly binding to SHR and/or SCR [15,16]. Our further analysis of this region using purified proteins of MGP ZFs showed that ZF4 is essential for binding to the SHR-SCR complex and ZF3-ZF4 exhibited comparable affinity to that of ZF1-ZF4 (Fig. 4a, b, Supplementary Fig. 5c). Our isothermal titration calorimetry (ITC) showed relatively high affinity of the SHR-SCR complex to MGP ZF3-ZF4 (the K_D value of 36 nM) and JKD ZF3-ZF4 (124 nM) (Fig. 4c, d). The complex between the SHR-SCR complex and ZF3-ZF4 exists as a stable heterotrimer in solution (Fig. 4e). Our competition experiments using gel filtration chromatography and pull-down assay showed that addition of JKD induced dissociation of MGP from the MGP-SHR-SCR ternary complex and *vice versa* (Supplementary Fig. 7, 8), suggesting that the binding of JKD and MGP is exclusive, probably because of the overlapped binding sites for JKD and MGP.

Zinc fingers responsible for DNA binding

Eukaryotic ZF transcription factors usually contain tandem repeats of ZF motifs, although not all ZF repeats are required for DNA binding. In fact, the presence of more than three repeats did not dramatically enhance the affinity to DNA [25]. We analyzed the DNA binding affinity of different ZF repeats of MGP using a fluorescence polarization assay. JKD and MGP bind the consensus DNA sequence, which was initially identified as a binding sequence for maize IDD protein ID1 [26,27]. Our DNA binding assay using this consensus sequence with ZFs of MGP showed high affinity (K_D value of 50 nM) for ZF1-4 (all four ZFs) (Fig. 4f). ZF1-ZF3 exhibited comparable high affinity (71 nM), indicating that ZF4 is not important for DNA binding. In contrast to ZF4, ZF1 is critical for DNA binding because the affinity of ZF2-ZF4 was reduced (289 nM). ZF2 alone exhibited low affinity (6.7 μM), but ZF2-ZF3 partially recovered the DNA binding affinity (562 nM). In contrast to this observed recovery of affinity, ZF3-ZF4 exhibited the lowest affinity (48 μM), suggesting that linked ZF2-ZF3 is important for DNA binding, unlike the ZF3-ZF4 link. Taken together, the three ZFs, ZF1-ZF2-ZF3, should be important for DNA binding, and ZF3 is expected to participate in two interactions, comprising binding to DNA and to SHR-SCR.

Structure of the JKD-SHR-SCR complex reveals the ZF-binding groove of SHR

The crystal structure of the SHR-SCR complex bound to JKD ZF3-ZF4 was successfully determined at 2.7Å resolution (Supplementary Table 1). Each ZF of JKD is folded into a common ββα-type structure, in which a short α-helix sits on an antiparallel β-sheet, by coordinating to a zinc ion as found for a classical C_2HC zinc-finger (Fig. 5a, Supplementary Fig. 9). The JKD ZFs bind SHR, whereas no contacts were found with SCR (Fig. 5b, Supplementary Fig. 10a). On JKD binding, no significant conformational changes are induced in the SHR-SCR heterodimer (Supplementary Fig. 10b). The JKD ZFs dock into the groove on the α/β core subdomain of SHR with an interface of 913 $Å^2$ (Fig. 5b). The groove, hereafter referred to as the ZF-binding groove, comprises three surface α-helices (α7, α4 and α13) with two helices (α5 and α6) at the bottom of the groove (Fig. 5b). The orientation of the two ZFs of JKD against the groove differ: the α-helix of ZF4 is docked into the groove, whereas the β-sheet of ZF3 faces the groove. Docking of the ZF4 α-helix is stabilized by deep insertion of Phe206 and other nonpolar residues (Ile201, Thr202, Ala205) into the groove (Fig. 5c) and formation of a salt bridge (Asp208 with SHR Arg222) and other electrostatic interactions (Fig. 5d). In contrast to these multiple contacts of ZF4, ZF3 is involved in only a few direct contacts with SHR, comprising electrostatic interactions *via* the β-sheet. Mutational studies support the importance of these two ZFs and nonpolar/polar residues interacting with the groove (Fig. 5e).

The SHR-binding motif is widely conserved in the BIRD/IDD family

We identified the conserved sequence R(K/R)DxxITHxAFCD (in which x represents any residue) of the ZF4 α-helix as the “SHR-binding motif (SHBM)” essential for SHR binding (Fig. 6a). The SHR-binding motif is ZF4-specific and similar sequences are absent in ZF1, ZF2 and ZF3 (Supplementary Fig. 9b). More importantly, this motif is highly conserved in 13 (from IDD1 to IDD13) out of 16 members of the *Arabidopsis thaliana* BIRD/IDD family of transcription factors [13] (Supplementary Fig. 6). In contrast to this high similarity, the other three members (IDD14, IDD15 and IDD16) lack a Phe residue corresponding to Phe206 of JKD ZF4, and other residues important for SHR binding. It is also noteworthy that the SHR residues responsible for JKD binding are less conserved in other GRAS proteins, suggesting specific binding to SHR but not to other GRAS family proteins (Supplementary Fig. 1a). Taken together, we speculate that BIRD/IDD family members could be categorized into two groups, comprising SHR-binding members (IDD1-13) and others (IDD14-16) displaying no SHR binding.

A DNA-binding model of the BIRD transcription factor in complex with the SHR-SCR complex

It is well established that the α-helix of ββα-type ZFs docks into the major groove of DNA for reading of the DNA sequence [25]. This dogma is consistent with our ternary structure, in which the ZF3 α-helix faces the outside and could be accessible to DNA binding, while the ZF4 α-helix is buried within the SHR groove and would be inaccessible to DNA binding. The mouse immediate early protein Zif268 is a typical ZF transcription factor containing three tandem repeats of C_2H_2 ZFs. The crystal structure of the DNA-bound form showed that each ZF is folded into a typical ββα structural module, which is docked into the major

groove of DNA in a configuration with the ZF α-helix inside the groove and the β-sheet outside the groove [28]. This binding mode enabled us to easily fit JKD ZF3-ZF4 bound to the SHR-SCR complex to the Zif268 ZFs bound to DNA. Our structural alignment using the Zif268 structure suggests that DNA-bound JKD ZFs can also bind the SHR-SCR complex by fitting JKD ZF3 to the ZF3 of Zif268 (Fig. 6b). Our electrophoretic mobility shift assay (EMSA) showed DNA binding of MGP ZF1-4 and JKD ZF1-4 were virtually unchanged in the presence or absence of the SHR-SCR complex (Fig. 6c). Additionally, SHR/SCR binding to MGP and JKD did not interfere with DNA binding, which further supports our model. In conclusion, of the four ZFs of MGP and possibly JKD, ZF1, ZF2 and ZF3 are responsible for DNA binding, while ZF3 and ZF4 are involved in SHR binding. These results suggest that SHR-SCR are transcriptional cofactors that regulate target gene transcription *via* binding of SHR to BIRD transcription factors.

Discussion

The GRAS proteins are plant-specific and are encoded by a large gene family; 33 and 66 GRAS members are present in the *Arabidopsis* and rice genomes, respectively [19]. A number of GRAS proteins have been shown to play key roles in regulating diverse processes [19,29]. Our study revealed that the GRAS domains of SHR and SCR each comprise an α-helical cap and α/β core subdomains, which is similar to the recently reported structure of SCARECROWLIKE7 in rice (OsSCL7) (Supplementary Fig. 11) [30]. In general, the GRAS domain shows structural similarity with SAM-MT α/β enzymes. This structural similarity is reminiscent of GA receptor GID1, which is folded into another α/β hydrolase fold and the α-helical lid interacts with DELLA proteins [20]. Moreover, strigolactone receptor D14 is also folded into another α/β hydrolase fold [31,32].

Our *in vitro* experiments showed that SHR or SCR alone tended to form aggregates or precipitates. We speculate that this phenomenon is caused by the α-helical cap, which may be conformationally unstable in the absence of binding partner and tends to make non-specific interactions that result in aggregate formation. We found, however, that two other *Arabidopsis* GRAS proteins AtSCL3 and AtSCL5 each exist in a stable form in solution: our AUC analysis suggested that AtSCL3 exists as a homodimer, while AtSCL5 exists as a monomer (Supplementary Fig. 12). In addition, OsSCL7 forms a homodimer [30]. These findings suggest that there are subtypes of GRAS proteins with different physical properties as determined by the α-helical caps, which mediate hetero- and/or homo-dimerization, or the absence of dimerization altogether.

In addition, the dimerization interfaces of different GRAS proteins may also be distinct. Our study shows that SHR-SCR forms a heterodimer *via* their α-helical caps in a head-to-head configuration, which is mediated by both polar and non-polar specific interactions. However, OsSCL7 was shown to form a homodimer in a side-by-side configuration mainly *via* hydrophobic interactions, with creation of a putative DNA binding groove at the dimer interface [30]. Although GRAS proteins function in transcriptional regulation, only two GRAS proteins, OsSCL7 and Nodulation Signaling Pathway1 (NSP1) in *Medicago truncatula*, have been reported to bind DNA directly by EMSA analysis [29,30]. In contrast, there is no evidence for direct binding of SHR-SCR or other GRAS proteins to DNA. We did not find

any DNA-binding motifs in our structure of the SHR-SCR complex, which comprises an overall negatively-charged surface potentials (Fig. 6d, *bottom*), which are unfavorable for binding to highly negatively-charged DNA. Our structure analysis of the JKD-SHR-SCR complex further supports that SHR-SCR play a role as transcription cofactors, which bind to target genes indirectly *via* the interacting BIRD transcription factors (e.g. JKD). Therefore, GRAS proteins may function as transcription factors or transcription cofactors.

The fourth Zinc finger ZF4 of BIRD transcription factors is critical for SHR binding and conserve the SHBM sequence, which provides an useful clue to understand the networking of these transcription factors with SHR and its binding partner SCR [16]. Moreover, SCR also possesses a deep groove corresponding to the JKD ZF-binding groove of SHR, although the SCR groove is less charged than that of SHR (Fig. 6c, *top*). We speculate that SCR and probably other GRAS domain proteins interact with their partner proteins *via* their grooves. Recent reports suggested that other GRAS family proteins, SCL3 and DELLA proteins exclusively bind to BIRDs/IDDs and play an antagonistic role in GA signalling[33,34]. In these studies, SCL3 or DELLA GRAS domain have been proposed to interact with the C-terminal region of BIRDs/IDDs rather than N-terminal zinc fingers responsible for SHR binding in the present study, suggesting that DELLA-mediated BIRDs/IDDs interaction is different from SHR-mediated interaction. Further structural studies of additional GRAS proteins and their interacting proteins will clarify the function of the grooves of GRAS proteins.

Methods

Protein expression and purification

The cDNAs of *Arabidopsis thaliana* SHR, SCR, MGP/IDD3 and JKD/IDD10 were obtained from RIKEN BioResource Center and transformed into *Escherichia coli* strain BL21Star (DE3) (Invitrogen) cells for protein expression. In our crystallization screening, we tried several protein constructs with different lengths by truncation of non-conserved flexible N- and/or C-terminal regions. Selenomethione (SeMet)-labelled SHR and SCR were prepared in M9 medium [35]. Detailed procedure is given in Supplementary Information 1.

Crystallization and data collection

Initial crystallization screening was performed using a Hydra II Plus One crystallization robot (Matrix Technology). X-ray diffraction data were collected on BL41XU or BL44XU beamlines at SPring-8. All data were processed and scaled using *HKL-2000* [36]. The crystal data are summarized in Supplementary Table 1. Detailed procedure is given in Supplementary Information 2.

Structure determination and refinement

Phases of the SHR-SCR complex crystal were calculated by a single-wavelength anomalous dispersion (SAD) method using data collected at the peak wavelength of selenium. Selenium positions were located using the program SHELXD [37], then phase calculation and refinement were performed with SHARP/autoSHARP [38]. One SHR-SCR complex is present in the asymmetric unit of the crystal. The built model was refined through alternating cycles using the Coot [39] and PHENIX [40] programs. The structure of the ternary complex of SHR

(113-531), SCR (275-653) and JKD/IDD10 (155-224) was determined by molecular replacement using the structure of a binary complex of SHR (59-531) and SCR (275-653) as a starting model. Molecular replacement was performed with Phaser [41]. Model building and refinement were performed as well as those for the SHR-SCR complex structure. The refinement statistics are summarized in Supplementary Table 1. The crystal contains two crystallographically independent ternary complexes in the asymmetric unit, which display similar structure with rms deviations based on Cα atoms of 0.39 Å (JKD), 0.24 Å (SHR) and 0.23 Å (SCR). Detailed description is given in Supplementary Information 1.

Structure and sequence comparison

Multiple sequence alignments of the GRAS domains and IDD family proteins were performed using CLUSTALW [42]. Pairwise structural comparisons were performed using C_α-atom positions by the DALI lite server [43] and structure figures were prepared using the PyMOL Molecular Graphics System, Version 1.7 Schrödinger, LLC (http://www.pymol.org/).

Analytical ultracentrifugation (AUC)

Sedimentation velocity ultracentrifugation experiments were performed at 20°C using a Beckman Coulter Optima XLA analytical ultracentrifuge. Purified samples were dissolved in 20 mM Tris buffer (pH 8.0) containing 150 mM NaCl. The resultant data were analyzed using the programs SEDFIT and SEDNTERP.

Binding studies by isothermal titration calorimetric analysis (ITC)

ITC was conducted using a calorimeter (iTC200, GE Healthcare) at 20°C. Purified protein samples were dialyzed overnight in buffer containing 20 mM Tris-HCl (pH 8.0) and 150 mM NaCl. We performed data fitting with a 1:1 binding model using the ORIGIN™ software program supplied with the instrument. The ITC profile (Fig. 4c) for binding of the SHR-SCR complex to the ZF3-ZF4 (ZF34) of MGP was obtained by injections of 6 μl of 626 μM MGP ZF34 (residues 143-221) into the SHR-SCR solution (94 μM) at 20°C. Raw data for 20 sequential injections (the upper panel) and the plot of the heat evolved (kcal) per mole of MGP ZF34 added, corrected for the heat of MGP ZF34 by dilution, against the molar ratio of MGP ZF34 to the SHR-SCR complex. The ITC profile (Fig. 4d) for binding of the SHR-SCR complex to the ZF34 of JKD was obtained by injections of 6 μl of 1.9 mM JKD ZF34 (155-224) into the SHR-SCR solution (100 μM) at 20°C.

Fluorescence polarization assay

5′-end Alexa488-labelled oligonucleotide (5′-GCTTTCTACTACCAAACCTTTT-3′) and its complement (5′-AAAAGGTTTGGTAGTAGAAAAGC-3′) were purchased from Invitrogen. These were mixed at an equal molar ratio and annealed to generate an IDD binding sequence. For the binding assay, the IDD binding sequence at a final concentration of 100 nM was mixed with MGP/IDD3 protein at a final concentration from 0 to 50 μM and incubated for 30 min at 20°C. The fluorescence polarization value of each sample was measured using a fluorescence polarization instrument (BEACON 2000, PanVera) equipped

with a 490 nm excitation filter and a 530 nm emission filter. Data were analyzed with the GraphPad Prism software program.

Electrophoretic mobility shift assay

5 μM of DNA prepared as described in above was mixed with 10 μM of indicated proteins in the buffer containing 20 mM Tris-HCl (pH7.5), 150 mM NaCl, 1 mM TCEP and 10 μM $ZnCl_2$. After incubation for 30 min at 20°C, the samples were subjected on native polyacrylamide gel electrophoresis with TAE buffer followed by image analysis (LAS4000, GE healthcare).

Pull-down binding assay

All mutations were produced by site-directed mutagenesis. For *in vitro* pull-down binding assays, the purified protein and GST-fusion protein were mixed with a slurry of glutathione-Sepharose 4B and incubated at 4°C. After washing with incubation buffer, collected eluates were subjected to SDS-PAGE. In the analysis of SHR-SCR interaction (Fig. 3f), MBP fused SHR GRAS domain (WT and mutants) were co-expressed with GST-SCR in *E. coli* and the lysate was applied to a glutathione sepharose resin. After washing several times, eluates were collected and then subjected to SDS-PAGE and western blotting with anti-MBP antibody (New England Biolabs). The relative amount of pulled down MBP-SHR is shown at the bottom with error bars representing standard deviation from three independent measurements (bottom panel). In the analysis of the interactions between MGP and the SHR-SCR complex (Fig. 4b), GST-MGP was pulled down from a mixture of GST-MGP and the complex between SHR and MBP-SCR. The MBP-SCR fusion protein was used to avoid band overlap in the PAGE. The relative amount of SHR pulled down was measured with error bars representing standard deviation from three independent measurements.

In vivo co-immunoprecipitation assay

C-terminal FLAG tagged *SCR* and N-terminal yellow florescent protein Venus [44] tagged *SHR* variants were independently cloned into pBI121 vector (Clontech). For enhancing the protein expression, Tomato bushy stunt virus *p19* gene was used for silencing suppressor [45]. Each construct was transformed into *Agrobacterium tumefaciens* GV3101 (pMP90) and infiltrated into *Nicotiana benthamiana* leaves for co-expression. Detailed procedure is given in Supplementary Information 3.

Data availability

Structural data that support the findings of this work have been deposited to Protein Data Bank with the following accession numbers: the SHR-SCR complex (5B3G) and the JKD-SHR-SCR complex(5B3H).

Supplementary Material

Refer to Web version on PubMed Central for supplementary material.

Acknowledgments

We thank R. Kurata for technical support in performing the MALDI-TOF MS analysis. We appreciate access to BL41XU and BL44XU beamlines at the SPring-8 synchrotron facility for the provision of synchrotron data-collection facilities (proposal nos.2013A6844, 2013B1288, 2013B6844, 2014A 1283 and 2014A6944). The cDNAs were provided by RIKEN BRC through the National Bio-Resource Project of the MEXT, Japan. This work was supported by a Grant-in-Aid for Scientific Research on Innovative Areas “Structural Cell Biology” (to T.H.), a Grant-in-Aid for Scientific Research (C) (to Y.H.) from MEXT, Japan, and the National Institutes of Health, US (R01 GM100051 to T.P.S.).

References

1. Pauluzzi G, et al. Surfing along the root ground tissue gene network. Dev Biol. 2012; 365:14–22. [PubMed: 22349629]
2. Petricka JJ, Winter CM, Benfey PN. Control of Arabidopsis root development. Annu Rev Plant Biol. 2012; 63:563–590. [PubMed: 22404466]
3. Benfey PN, et al. Root development in Arabidopsis: four mutants with dramatically altered root morphogenesis. Development. 1993; 119:57–70. [PubMed: 8275864]
4. Scheres B, et al. Mutations affecting the radial organisation of the Arabidopsis root display specific defects throughout the embryonic axis. Development. 1995; 121:53–62.
5. Di Laurenzio L, et al. The SCARECROW gene regulates an asymmetric cell division that is essential for generating the radial organization of the Arabidopsis root. Cell. 1996; 86:423–433. [PubMed: 8756724]
6. Helariutta Y, et al. The SHORT-ROOT gene controls radial patterning of the Arabidopsis root through radial signaling. Cell. 2000; 101:555–567. [PubMed: 10850497]
7. Sabatini S, Heidstra R, Wildwater M, Scheres B. SCARECROW is involved in positioning the stem cell niche in the Arabidopsis root meristem. Genes Dev. 2003; 17:354–358. [PubMed: 12569126]
8. Cui H, Kong D, Liu X, Hao Y. SCARECROW, SCR-LIKE 23 and SHORT-ROOT control bundle sheath cell fate and function in Arabidopsis thaliana. Plant J. 2014; 78:319–327. [PubMed: 24517883]
9. Nakajima K, Sena G, Nawy T, Benfey PN. Intercellular movement of the putative transcription factor SHR in root patterning. Nature. 2001; 413:307–311. [PubMed: 11565032]
10. Heidstra R, Welch D, Scheres B. Mosaic analyses using marked activation and deletion clones dissect Arabidopsis SCARECROW action in asymmetric cell division. Genes Dev. 2004; 18:1964–1969. [PubMed: 15314023]
11. Cui H, et al. An evolutionarily conserved mechanism delimiting SHR movement defines a single layer of endodermis in plants. Science. 2007; 316:421–425. [PubMed: 17446396]
12. Levesque MP, et al. Whole-genome analysis of the SHORT-ROOT developmental pathway in Arabidopsis. PLoS Biol. 2006; 4:e143. [PubMed: 16640459]
13. Colasanti J, et al. The maize INDETERMINATE1 flowering time regulator defines a highly conserved zinc finger protein family in higher plants. BMC Genomics. 2006; 7:158. [PubMed: 16784536]
14. Sozzani R, et al. Spatiotemporal regulation of cell-cycle genes by SHORTROOT links patterning and growth. Nature. 2010; 466:128–132. [PubMed: 20596025]
15. Welch D, et al. Arabidopsis JACKDAW and MAGPIE zinc finger proteins delimit asymmetric cell division and stabilize tissue boundaries by restricting SHORT-ROOT action. Genes Dev. 2007; 21:2196–2204. [PubMed: 17785527]
16. Long Y, et al. Arabidopsis BIRD Zinc Finger Proteins Jointly Stabilize Tissue Boundaries by Confining the Cell Fate Regulator SHORT-ROOT and Contributing to Fate Specification. Plant Cell. 2015; 27:1185–1199. [PubMed: 25829440]
17. Moreno-Risueno MA, et al. Transcriptional control of tissue formation throughout root development. Science. 2015; 350:426–430. [PubMed: 26494755]
18. Pysh LD, Wysocka-Diller JW, Camilleri C, Bouchez D, Benfey PN. The GRAS gene family in Arabidopsis: sequence characterization and basic expression analysis of the SCARECROW-LIKE genes. Plant J. 1999; 18:111–119. [PubMed: 10341448]

19. Bolle C. The role of GRAS proteins in plant signal transduction and development. Planta. 2004; 218:683–692. [PubMed: 14760535]
20. Murase K, Hirano Y, Sun TP, Hakoshima T. Gibberellin-induced DELLA recognition by the gibberellin receptor GID1. Nature. 2008; 456:459–463. [PubMed: 19037309]
21. Sun X, Jones WT, Rikkerink EH. GRAS proteins: the versatile roles of intrinsically disordered proteins in plant signalling. Biochem J. 2012; 442:1–12. [PubMed: 22280012]
22. Gallagher KL, Benfey PN. Both the conserved GRAS domain and nuclear localization are required for SHORT-ROOT movement. Plant J. 2009; 57:785–797. [PubMed: 19000160]
23. Martin JL, McMillan FM. SAM (dependent) I AM: the S-adenosylmethionine-dependent methyltransferase fold. Curr Opin Struct Biol. 2002; 12:783–793. [PubMed: 12504684]
24. Joshi CP, Chiang VL. Conserved sequence motifs in plant S-adenosyl-L-methionine-dependent methyltransferases. Plant Mol Biol. 1998; 37:663–674. [PubMed: 9687070]
25. Pabo CO, Peisach E, Grant RA. Design and selection of novel Cys2His2 zinc finger proteins. Annu Rev Biochem. 2001; 70:313–340. [PubMed: 11395410]
26. Kozaki A, Hake S, Colasanti J. The maize ID1 flowering time regulator is a zinc finger protein with novel DNA binding properties. Nucleic Acids Res. 2004; 32:1710–1720. [PubMed: 15020707]
27. Ogasawara H, Kaimi R, Colasanti J, Kozaki A. Activity of transcription factor JACKDAW is essential for SHR/SCR dependent activation of SCARECROW and MAGPIE and is modulated by reciprocal interactions with MAGPIE, SCARECROW and SHORT ROOT. Plant Mol Biol. 2011; 77:489–499. [PubMed: 21935722]
28. Pavletich NP, Pabo CO. Zinc finger-DNA recognition: crystal structure of a Zif268-DNA complex at 2.1 Å. Science. 1991; 252:809–817. [PubMed: 2028256]
29. Hirsch S, et al. GRAS proteins form a DNA binding complex to induce gene expression during nodulation signaling in Medicago truncatula. Plant Cell. 2009; 21:545–557. [PubMed: 19252081]
30. Li S, et al. Crystal structure of the GRAS domain of SCARECROW-LIKE 7 in Oryza sativa. Plant Cell. 2016; 28:1025–1034. [PubMed: 27081181]
31. Hamiaux C, et al. DAD2 is an α/β hydrolase likely to be involved in the perception of the plant branching hormone, strigolactone. Curr Biol. 2012; 22:2032–2036. [PubMed: 22959345]
32. Kagiyama M, et al. Structures of D14 and D14L in the strigolactone and karrikin signaling pathways. Genes Cells. 2013; 18:147–160. [PubMed: 23301669]
33. Yoshida H, et al. DELLA protein functions as a transcriptional activator through the DNA binding of the INDETERMINATE DOMAIN family proteins. Proc Natl Acad Sci U S A. 2014; 111:7861–7866. [PubMed: 24821766]
34. Fukazawa J, et al. DELLAs function as coactivators of GAI-ASSOCIATED FACTOR1 in regulation of gibberellin homeostasis and signaling in Arabidopsis. Plant Cell. 2014; 26:2920–2938. [PubMed: 25035403]
35. Doublie S. Preparation of selenomethionyl proteins for phase determination. Methods Enzymol. 1997; 276:523–530.
36. Otwinowski Z, Minor W. Processing of X-ray diffraction data collected in oscillation mode. Methods Enzymol. 1997; 276:307–326.
37. Schneider TR, Sheldrick GM. Substructure solution with SHELXD. Acta Crystallogr. 2002; D58:1772–1779.
38. Vonrhein C, Blanc E, Roversi P, Bricogne G. Automated structure solution with autoSHARP. Methods Mol Biol. 2007; 364:215–230. [PubMed: 17172768]
39. Emsley P, Cowtan K. Coot: model-building tools for molecular graphics. Acta Crystallogr. 2004; D60:2126–2132.
40. Adams PD, et al. PHENIX: a comprehensive Python-based system for macromolecular structure solution. Acta Crystallogr. 2010; D66:213–221.
41. McCoy AJ, et al. Phaser crystallographic software. J Appl Cryst. 2007; 40:658–674. [PubMed: 19461840]
42. Larkin MA, et al. Clustal W and Clustal X version 2.0. Bioinformatics. 2007; 23:2947–2948. [PubMed: 17846036]

43. Holm L, Park J. DaliLite workbench for protein structure comparison. Bioinformatics. 2000; 16:566–567. [PubMed: 10980157]

44. Nagai T, et al. A variant of yellow fluorescent protein with fast and efficient maturation for cell-biological applications. Nat Biotechnol. 2002; 20:87–90. [PubMed: 11753368]

45. Shimura H, et al. A strategy for screening an inhibitor of viral silencing suppressors, which attenuates symptom development of plant viruses. FEBS Lett. 2008; 582:4047–4052. [PubMed: 18996375]

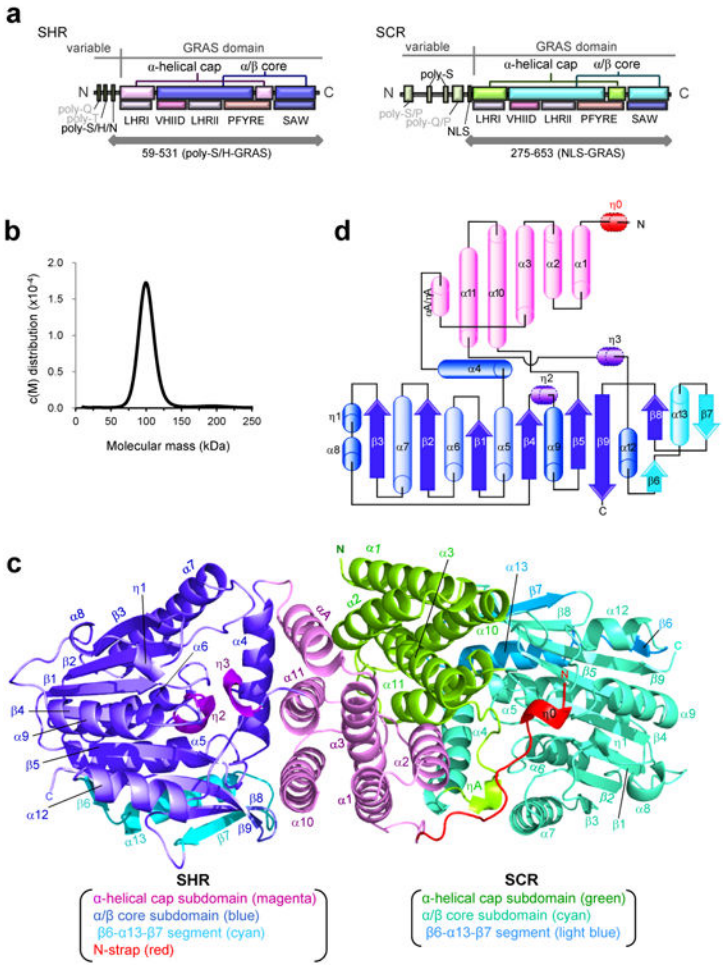

Figure 1. Structure of the heterodimeric SHR-SCR complex

a, Domain maps of SHR and SCR. The GRAS domain comprises LHRI, VHIID, LHRII, PFYRE and SAW modules. SHR possesses a relatively short N-terminal variable region (residues 1-135) containing Gln, Thr and Ser/His/Asn repeats (poly-Q, poly-T and poly-S/H/N), while SCR possesses a longer N-terminal variable region (1-280) containing Ser/Pro, Ser and Gln/Pro repeats (poly-S/P, poly-S, poly-Q/P) and a nuclear localization signal (NLS).Both are predicted to comprise intrinsically disordered regions without apparent secondary structures.

b, Distribution of apparent molecular mass of the SHR-SCR complex obtained from sedimentation velocity analysis. The observed mono-dispersed state with an estimated molecular mass of 105.4 ± 1.4 kDa suggests a heterodimer in solution (calculated mass 89.2 kDa).

c, Ribbon representation of the crystal structure of the heterodimer of SHR and SCR GRAS domains. SHR comprises the N-terminal strap (in red), α-helical cap (magenta) and α/β core (blue) subdomain, while SCR consists of the α-helical cap (green) and α/β core (cyan). The α/β core subdomains contain GRAS-specific segments, β6-α13-β7 (cyan in SHR and light blue in SCR, respectively). The N-terminal 6 residues of SCR (residues 275-280) and 61 residues of SHR (residues 59-119) were not observed in the current map. The overall

structure of the SCR GRAS domain resembles that of the SHR GRAS domain except for the replacement of αA-helix with a short 3_{10}-helix (ηA) and the absence of two 3_{10}-helices, η2 and η3.

d, Topology diagram of the GRAS domain of SHR. Color codes are as in **c**.

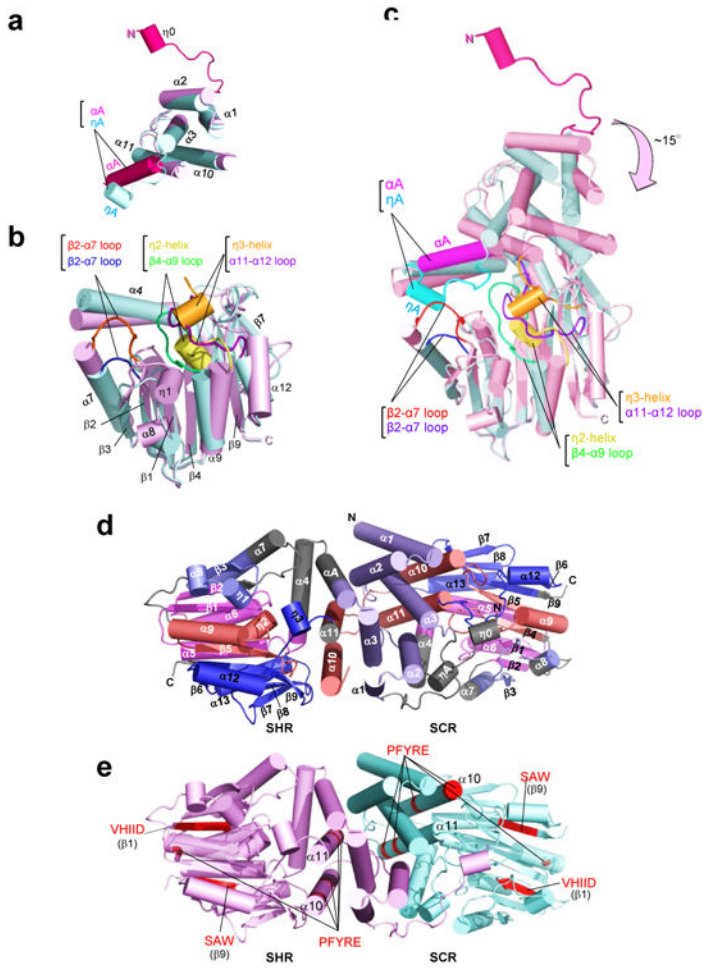

Figure 2. Structural comparison and GRAS conserved motifs

a, The α-helical caps of SHR and SCR superimpose with small root mean square (rms) deviation of 1.23 Å based on Ca atoms within 104 residues. A large structural deviation is found in αA helix (pink) of SHR and ηA helix (cyan) of SCR. The segments are indicated with labels for SHR (top) and SCR (bottom).

b, As in **a**, but for the α/β core subdomains with rms deviation of 1.69 Å (225 Ca atoms). Segments displaying large displacements are indicated with colored labels: (β2-α7 loop in red (SHR) / blue (SCR), η2 helix (SHR) in yellow / (β4-α9 loop (SCR) in green and η3 helix (SHR) in orange /η3 helix/α11-α12 loop (SCR) in purple.

c, As in **a**, but for the whole GRAS domains of SHR (pink) and SCR (cyan) with rms deviation of ~2.7 Å (350 C_α atoms). Compared with SHR, a swing (~15°) of the SCR α-helical cap against the a/β core is induced by structural deviations in αA helix, (β2-α7 loop and η2 and η3 helices at the boundary region between the α-helical cap and α/β core.

d, The modules LRI (purpleblue α1-α2-α3), VHIID (magenta α4-α5-(β1-α6-β2), LRII (cyan α7-p3-η1-α8), PFYRE (orange β4-(η2)-α9-β5-α10-α11) and SAW (blue (η3)-α12-β6-α13-β8-β9) are mapped on the SHR-SCR complex structure.

e, The conserved sequence motifs are mapped on the structure. The PFYRE motif contains Pro located at the α9-β5 loop, Phe and Tyr at α10 helix, and Arg and Glu at α11 helix.

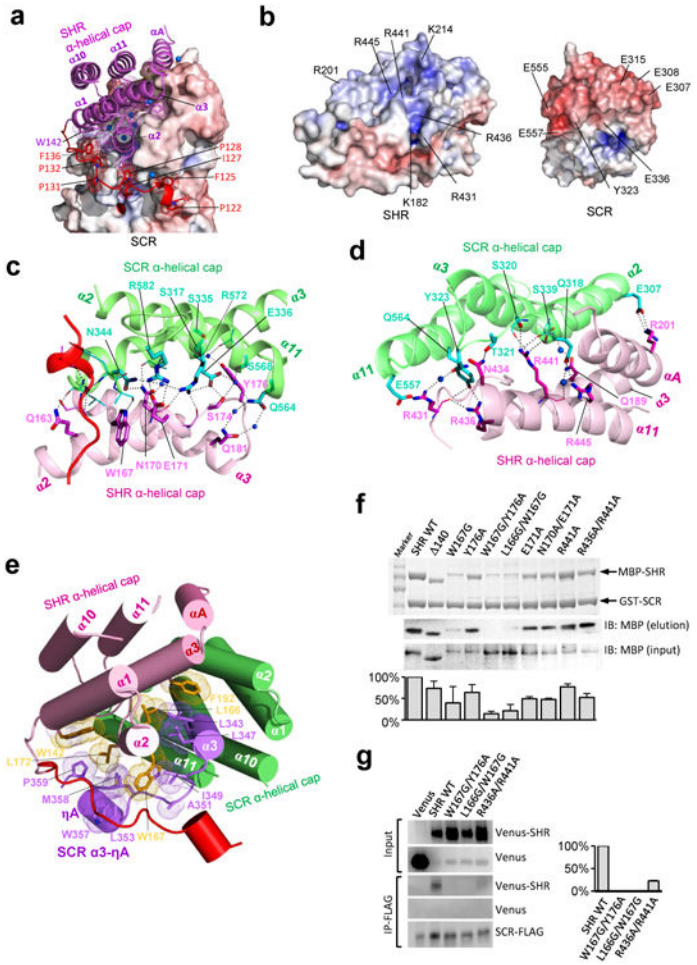

Figure 3. The SHR and SCR interaction

a, The α-helical cap helices (magenta ribbons) and the N-terminal strap (a red ribbon) of SHR bound to the SCR GRAS domain (electrostatic surface potentials with positive (blue) and negative (red) charges). The interface incorporates water molecules (blue balls).

b, The electrostatic surface potential of the SHR-SCR interface shown in an open book manner.

c, The interface between α2/α3 helices of SHR and α3/α11 helices of SCR incorporates both direct and water (blue balls)-mediated polar interactions (dotted lines).

d, As in **c**, but for the interface between α3/αA/α11 helices of SHR and α2/α3/α11 helices of SCR.

e, The SCR hydrophobic belt (α3-ηA loop, α3 and ηA helices in purple) possesses nonpolar residues (stick models with surface dots) contacting nonpolar residues (orange) from SHR by wrapping α2-helix of SHR

f, Pull-down binding assay. MBP fused SHR GRAS domain (WT and mutants) were pulled down with GST-SCR and analyzed by SDS-PAGE (top panel) with Western blotting with anti-MBP antibody (New England Biolabs) (middle panel) and quantification of the relative amount of pulled down MBP-SHR (bottom panel). Δ140 represents the 140-residues deletion containing the N-terminal variable region.

(**g**), *In vivo* co-immunoprecipitation assay. Wild-type (WT) or mutated Venus-SHR was co-immunoprecipitated with SCR-FLAG from protein extracts of *Nicotiana benthamiana* leaves, in which *SCR* with C-terminal FLAG tag and *SHR* variants with N-terminal Venus were co-expressed. Quantification of co-immunoprecipitaed Venus-SHR is shown in the right panel.

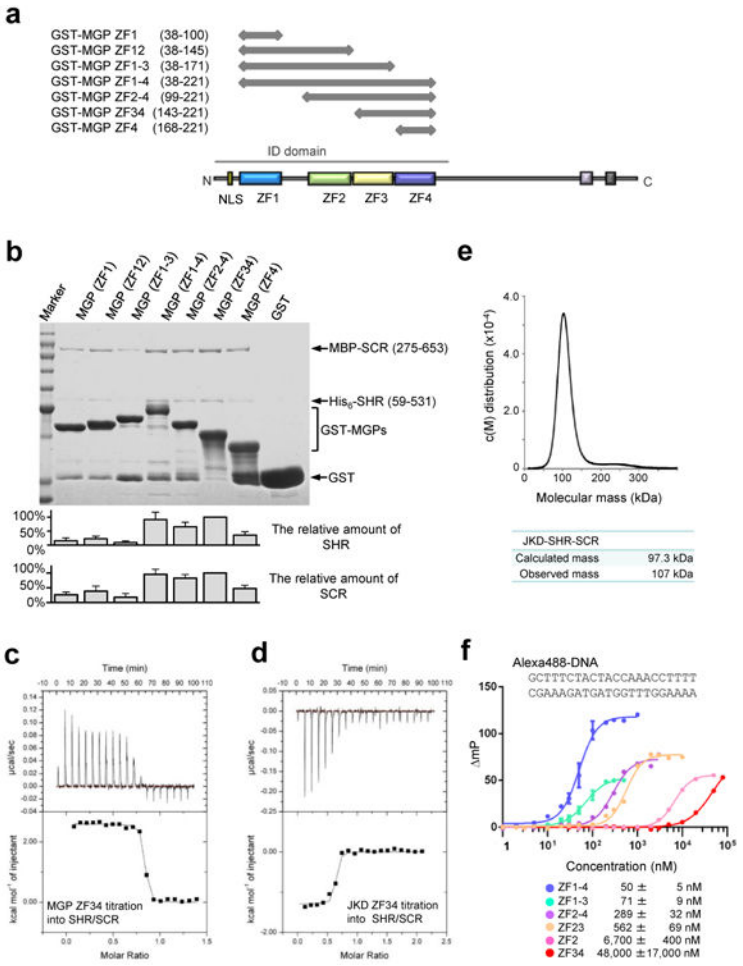

Figure 4. Zinc fingers of MGP and JKD essential for SHR-SCR binding and DNA binding

a, ZFs of GST-MGP proteins used for our *in vitro* pull-down binding assay.

b, *In vitro* pull-down binding assay. The SHR and MBP-SCR complex was pulled down with GST-MGP zinc fingers and analyzed by SDS-PAGE (upper panel). The relative amount of SHR and SCR pulled down are shown with error bars (bottom). Similar results were obtained from the SHR-SCR complex.

c, ITC profile for binding of the SHR-SCR complex to the ZF3-ZF4 (ZF34) of MGP. Theo btained K_D value is 35.5 ±11.2 nM, with ΔH, $T\Delta S$ and N values of 2.59 ± 0.02 kcal/mol, 12.6 kcal/mol and 0.81±0.003, respectively.

d, As in c, but for binding of the SHR-SCR complex to the ZF34 of JKD. The obtained K_D value is 123.8 ± 81.7 nM, with ΔH, $T\Delta S$ and N values of -1.29 ± 0.03 kcal/mol, 8.0 kcal/mol and 0.60 ± 0.01, respectively.

e, Distribution of apparent molecular mass of the JKD ZF34-SHR-SCR ternary complex obtained from sedimentation velocity analysis of AUC.

f, Fluorescence polarization of Alexa488-labelled DNA on binding to MGP. 100 nM of Alexa488-labelled DNA was mixed with various constructs of MGP at the indicated concentrations and the polarization (ΔmP) was plotted against MGP concentration.

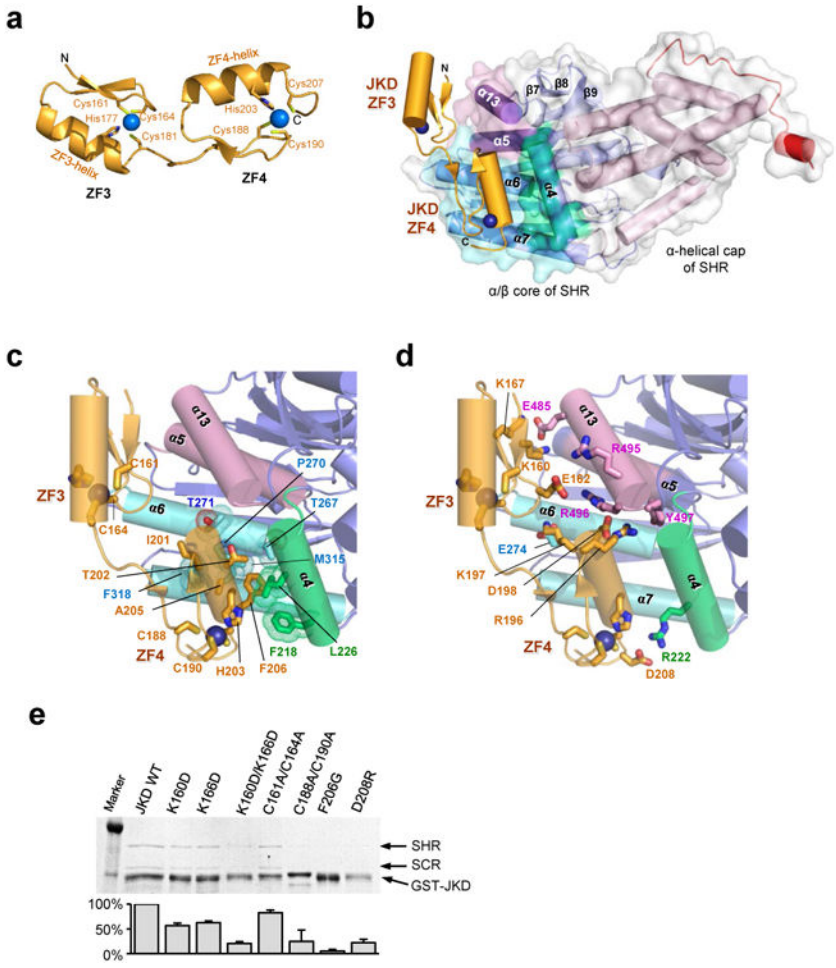

Figure 5. BIRD/IDD ZFs bind SHR of the SHR-SCR complex

(**a**) Ribbon model of the JKD ZF3-ZF4. Both ZF3 and ZF4 are folded into a typical ββα-type zinc finger structure with C_2HC ZF coordination to a zinc ion (blue ball). Side chains of the coordinated residues of ZF3 (Cys161, Cys164, His177 and Cys181) and ZF4 (Cys188, Cys190, His203 and Cys207) are shown as stick models.

(**b**) A ribbon diagram of JKD ZF34 (orange) bound to the α/β core of SHR in the JKD-SHR-SCR ternary complex with a surface model of the SHR GRAS domain (surface and cylinder model). The SCR GRAS domain is omitted for clarity given the absence of any interactions with JKD. JKD is surrounded by three walls of SHR shown in green (α4 helix), cyan (α6 and α7 helices) and magenta (α5 and α13 helices).

(**c**) A close-up view of intermolecular nonpolar interactions between JKD ZF34 and the binding groove on the α/β core of SHR.

(**d**) As in **c**, but for intermolecular electrostatic interactions between JKD ZF34 and the binding groove on the α/β core of SHR.

(**e**) Mutational analysis by *in vitro* pull-down assays using recombinant proteins. The SHR-SCR complex was pulled down with GST-JKD wild-type (JKD WT) or mutants on glutathione-Sepharose, and collected eluates were then subjected to SDS-PAGE. The relative

amount of SHR pulled down with GST-JKD constructs is shown with error bars representing standard deviation from three independent measurements

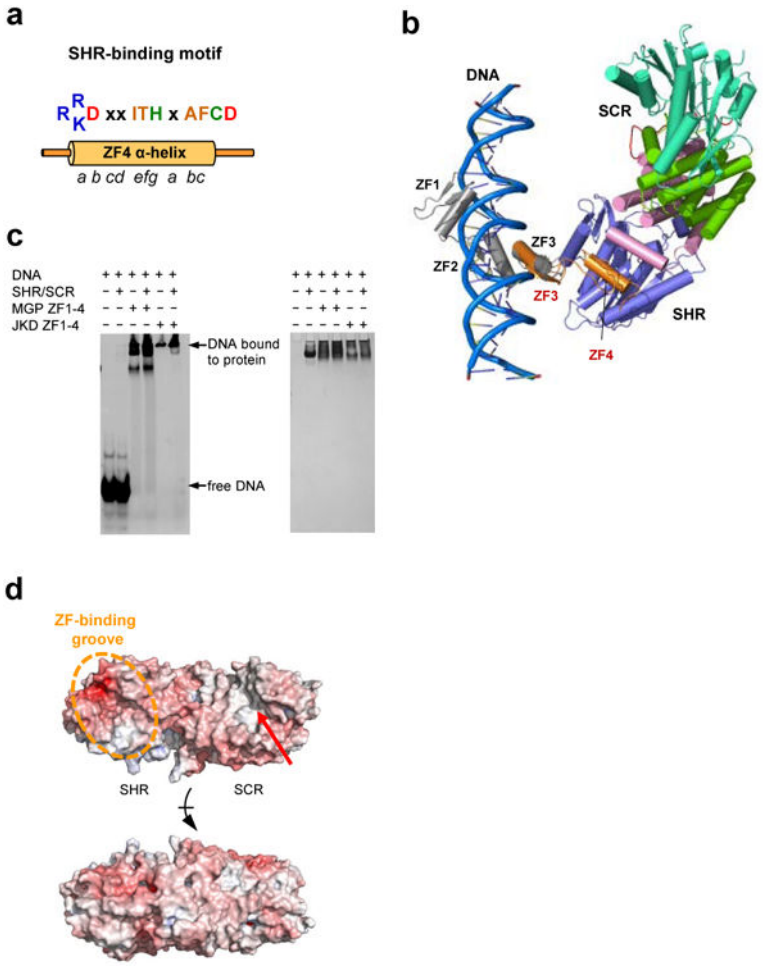

Figure 6. A DNA-bound model of the ZFs of BIRD/IDD transcription factors bound to the SHR-SCR complex

(**a**) The SHR-binding motif found in the α-helix of ZF4 of JKD. The motif is conserved in 13 members (IDD1-13) of the BIRD/IDD family of transcription factors. Each positional identifier of the heptad repeat (*abcdefg*) of α-helix is indicated from the N-terminus of the helix. The conserved residues IT at *ef* positions and AF at *bc* positions of the next repeat are located the nearly the same helix surface forming the interface with SHR on docking into the SHR groove.

(**b**) A model of the JKD-SHR-SCR ternary complex bound to DNA. JKD ZF3 was superimposed onto the ZF3 of Zif268 bound to DNA (gray, PDB code 1ZAA).

(**c**) EMSA with MGP or JKD in the presence or absence of SHR/SCR using Alexa488-labelled DNA. The left panel represented fluorescence image while the right panel represented a CBB stained gel.

(**d**) The JKD ZF34 binding groove (indicated with an orange circle) is shown on the electrostatic surface potential of the SHR-SCR complex (*top*). This surface is the backside of the surface depicted in Fig. 1c. A red arrow indicates the groove on SCR. The surface depicted in Fig. 1c is shown at the bottom.